

System Identification for Low-cost Small-scale Helicopters

Y. Reddi * E. Boje **

* *University of Cape Town, South Africa (e-mail:
rddyas002@myuct.ac.za)*

** *University of Cape Town, South Africa (e-mail:
Edward.Boje@uct.ac.za)*

Abstract: The preliminary platform design for a twin-helicopter slung load transportation system is presented. The framework is intended for testing robust multivariable control design methods and nonlinear state-estimation algorithms. An avionics unit is designed for on-board sensing and control. A low-cost visual tracking system is designed for estimating the helicopter pose within a flying volume. Using flight data logged by the avionics and visual tracking system, an uncertain set of parameters are estimated which completely define the plant dynamics for hover flight condition.

Keywords: System Identification, Parameter Estimation, Modelling, Helicopter, Visual Tracking and Robust Control

1. INTRODUCTION

The design of a coordinated load transportation system that consist of multiple helicopters present interesting and challenging engineering design problems. This non-trivial cross-coupled plant (shown in Fig. 1) was chosen as a platform for testing robust multivariable and load-sharing control system design techniques. The benefits of this scheme (in real-world applications) is that load lifting capacity may be increased and cost reduced by using multiple, lower-cost helicopters - instead of purpose-built heavy load lifting helicopters. In this paper, we discuss the design of a test-bed for the control system of a twin-helicopter slung load transportation system. Research interests in robust control methods such as H-infinity theory and Quantitative Feedback Theory (QFT) require well-defined plants, modelled with uncertainty. A high fidelity nonlinear model of a single helicopter (without attached load) is assembled and verified to capture the significant behaviour.

Multi-helicopter load lifting schemes were investigated by Bisgaard et al. (2009) and Bernard and Kondak (2009), with a focus on modelling and architecture design rather than robust control design. Bernard and Kondak (2009) present an adaptive multi-helicopter load lifting scheme. Bisgaard et al. (2009) developed a detailed model of the interaction between the helicopters in a multi-lift scheme and the load. In Mettler et al. (1999), a frequency domain based system identification method was applied to a small-size helicopter and linear model structure was arranged to capture the significant main rotor and stabilizer bar dynamics. Our experimental platform has been designed as a low-cost system for indoor use, hence the helicopters

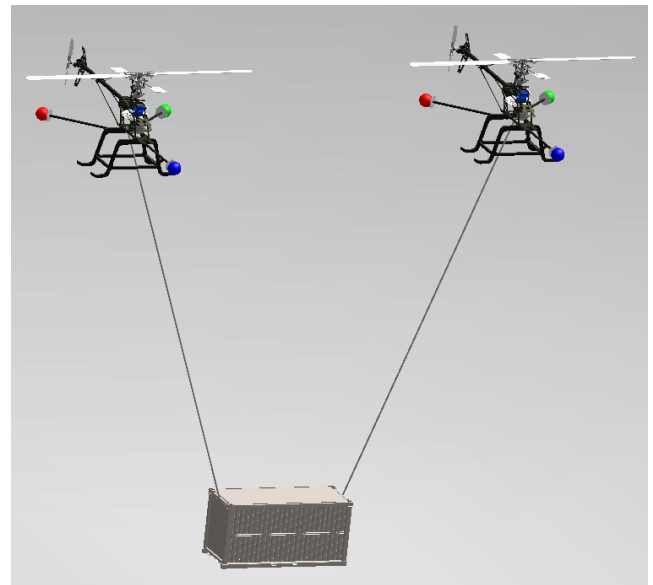


Fig. 1. Rendering of the twin-helicopter transportation system carrying a load

chosen are much smaller than that used in work referred to.

This paper presents the development of components of the laboratory system as follows. Section 2 discusses the instrumentation: Because of the small size of the helicopter, a light avionics board was developed for the project. For the system identification and control system implementation, a visual tracking system was designed from off-the-shelf components to estimate the position and attitude of the helicopters with accuracy and sample rate matching much more expensive commercially available systems. Section 3 presents the helicopter modelling; and Section 4 presents the system parameter identification based on

* Financial support from the University of Cape Town and the National Research Foundation is acknowledged.

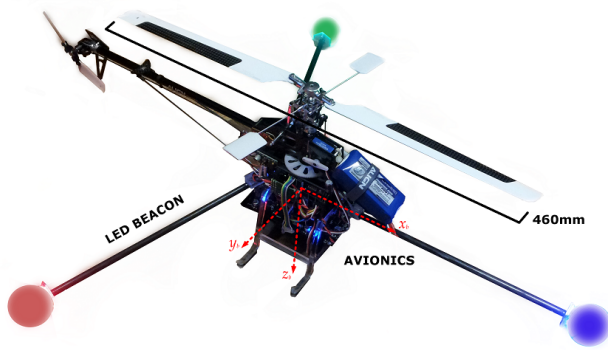


Fig. 2. Instrumented helicopter manually controlled flight tests. Concluding remarks are made in Section 5.

2. INSTRUMENTATION

Since the system was designed to be used indoors, a small electric radio controlled (RC) helicopter was chosen as the vehicle for the twin-helicopter slung load transportation system. The helicopters used are Align T-REX250SE with off-the-shelf specifications given in Table 1. The T-REX250SE has a Bell-Hiller rotor setup which has similar dynamics to a full-scale system, apart from the effect of the stabilizer bar according to Mettler et al. (1999). The higher rotor speed relative to the control loop bandwidth allows filtering of rotor induced vibrations in inertial sensors signals without significant phase-lag penalty. There are five inputs to the helicopter plant. The main rotor has three servos to alter lateral, longitudinal and collective pitch. A fourth servo is used to control the tail rotor pitch. The fifth input to the system is the speed command to the main rotor. The tail rotor is driven by a belt and gear system connected to the main rotor. The instrumented helicopter is shown in Fig. 2.

Table 1. Standard T-REX250SE Specifications

Characteristic	
Flying weight	340 g
Main rotor diameter	460 mm
Body length	430 mm
Hover main rotor speed	3500 rpm
Main to tail rotor gain	4.28

2.1 Avionics

Due to the small size of the helicopter, a custom avionics system weighing only 70 g was designed to provide for communication, motion/absolute position sensing, flight logging and fail-safe controls. It is shown in Fig. 3. To reduce the effect of vibration from the main rotor, the aerial application board is mounted with high density foam within the landing gear assembly. A description of the features are given below:

- **Sensors:** Include 3 axis gyroscope (ITG3200), accelerometer (ADXL345) and magnetometer (HMC5883) for body kinematics estimation. An ultrasonic distance sensor is used for altitude information (1 cm resolution). Geolocation for possible out-door flights can be obtained through the use of a GPS unit.

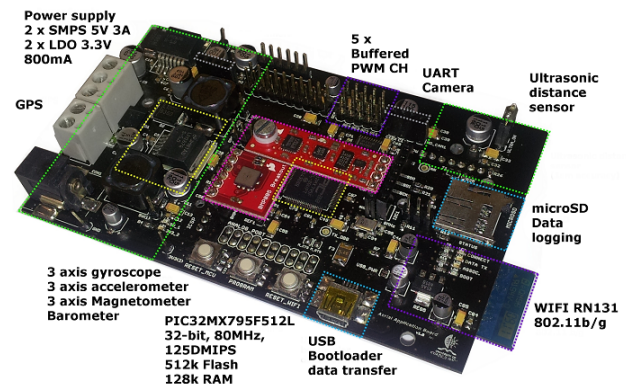


Fig. 3. Aerial application board highlighting key features

- **Communication:** WiFi technology is used for communication between the base station and the helicopter. A USB interface is available for fast streaming of data to a PC as well as for updating system firmware.
- **Storage:** A microSD card is used for logging flight data in real-time.
- **Processing:** The PIC32MX795F512L was chosen as the processing unit for performance versus power usage.

2.2 Motion Capture

Institutions famous for their coordinated high-speed quadrotor maneuvers, use costly off-the-shelf motion capture equipment, such as Vicon Motion Capture system (Ducard and D'Andrea (2009) and Mellinger et al. (2011)). For this project, we have developed a low-cost alternative to these systems that gives satisfactory reliability, resolution and frame rate for indoor aerial vehicle control.

The motion capture system consist of multiple camera/computer slave units and a master processing computer. The master and slaves communicate with each other over the network using TCP/IP. The computer/camera units run as servers on the network, servicing the master's requests. For simplicity in image processing, the platform that is to be tracked has markers that consist of a red, a green and a blue LED that form a coplanar triangle. White table tennis balls encase the LED's to diffuse the light. When pose estimation is required, the master issues a request to each slave. The slaves perform preprocessing of images and send a packet containing the number of each coloured blob, their respective image positions and a timestamp. Clock synchronization between master and slaves is achieved using Network Time Protocol (NTP) software. Once the master receives replies from all the slaves, it solves correspondence issues and performs the pose estimation of the platform in the scene.

The PSEye camera was chosen as the optical sensor in the motion capture system for its high frame rate (125 frames per second; resolution: 320x240) and low-cost. Four cameras, each located at a corner of the flying volume, provide sufficient coverage in the event of occlusions. Experimentation with the camera revealed that the USB interface bottlenecks the performance (in terms of latency and frame rate). A simple solution to this limitation was

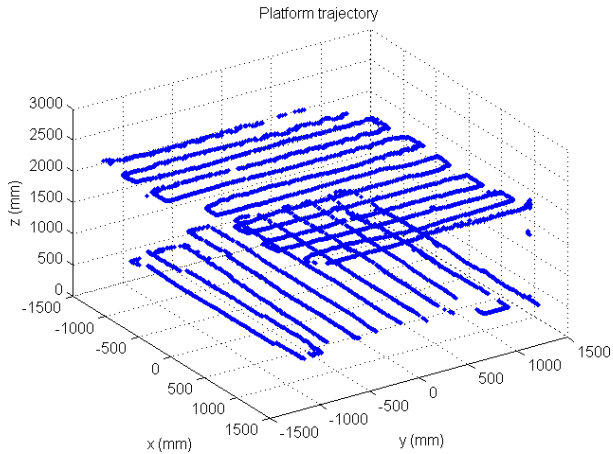


Fig. 4. Tracking experiment showing movement in flying volume

to use one low-specification computer per camera (in our case, discarded machines) with the view of migrating the slave software to low-end single board computers such as the Raspberry Pi for compactness and extensibility if required.

Results The platform was moved (manually) along a grid-like pattern to ensure that the tracking system is capable of locating the platform within the flying volume. The results of this test is shown in Fig. 4. The locations where discontinuities in the pattern exist is where the tracking system failed to locate the platform. The tracking region height is confined to $[0, 3]$ m, while the limits along the x -axis are $[-1.2, 1.5]$ m and y -axis are $[-1.2, 1.2]$ m.

The use of a *controlled* local network was found to minimise the variance in network delay. The worst-case latency of the system (including computation) was found to be 18 ms. The standard deviation of displacement error was found to be $\sigma = 0.4$ mm near the center of the room. The maximum frame rate possible with the current software is limited to 60 Hz. The tracking system gives results that are accurate and fast enough for outer-loop (position and attitude) feedback control of the twin-helicopter load transportation system.

3. NONLINEAR PLANT MODEL

A high fidelity model of a plant is required for *optimal* control design - optimal in the sense that the minimum control effort is made to meet the specifications for the uncertain plant set. Reduction in the scale of helicopters typically is accompanied by an increase in plant bandwidth (Mettler et al. (1999)) due to two significant factors: the reduction in mass and inertia of the body that results in higher bandwidth (low-pass) filtering of the body dynamics; and the reduction in the mass and inertia of the rotor blades, and the increase in rotor angular velocity that result in a reduced rotor time constant. The helicopter model is broken up into multiple sections shown in Fig. 5 following the modelling approach in Hald et al. (2006).

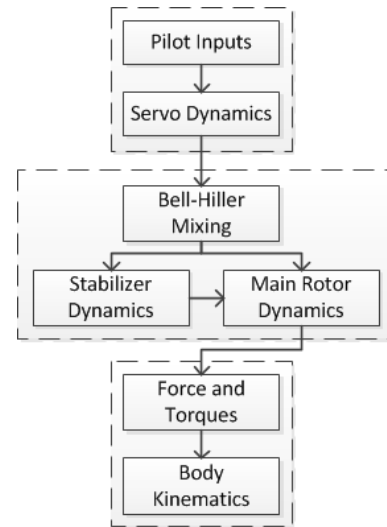


Fig. 5. High-level overview of the helicopter model

3.1 Plant Inputs and Servo Dynamics

The pilot control inputs denoted by $\mathbf{T} = [T_{lat}, T_{lon}, T_{col}, T_{yaw}]^T$, the lateral and longitudinal cyclic, main collective and tail collective controls respectively. The convention for these signals is shown in Table. 2. These signals are scaled via the mixing settings on the RC transmitter to control the range of actuation. The scaled signals are then mapped to the servo inputs. The T-REX250SE has a

Table 2. Pilot input convention

Signal (+ve)	Interpretation
T_{col}	Negative force in the body z-axis
T_{lat}	Negative body roll rate
T_{lon}	Negative body pitch rate
T_{yaw}	Positive body yaw rate

120° cyclic head system with three servos controlling the cyclic and collective movement. The pilot input signals are mapped to the servo signals via

$$\Delta_{servo} = \begin{bmatrix} \delta_{left} \\ \delta_{right} \\ \delta_{rear} \\ \delta_{rud} \end{bmatrix} = \begin{bmatrix} K_{col} & -K_{lat} & -K_{lon} & 0 \\ K_{col} & K_{lat} & -K_{lon} & 0 \\ K_{col} & 0 & 2K_{lon} & 0 \\ 0 & 0 & 0 & K_{rud} \end{bmatrix} \mathbf{T} \quad (1)$$

where K_{col} , K_{lat} , K_{lon} and K_{rud} are the pitch, lateral, longitudinal and rudder mixing gains respectively.

3.2 Bell-Hiller Mixing and Rotor Dynamics

A common feature among small-scale helicopters is the Bell-Hiller mixing system. This mechanism slows down the the main rotor dynamics and provides damping to body rate disturbances. The blade pitch angle in a Bell-Hiller mixing configuration is a function of the pilot inputs as well as the flapping angles of the stabilizer bar. The blade pitch as a function of the blade position (azimuth), with respect to the rear (clockwise rotation as positive) of the helicopter may be written as,

$$\theta_{mr}(\Psi) = T'_{col} - T'_{lat} \cos(\Psi) - T'_{lon} \sin(\Psi) \quad (2)$$

where T'_{col} is the collective blade pitch, T'_{lat} is the blade pitch due to a lateral command, and T'_{lon} is the blade

pitch due to a longitudinal command. The first harmonic approximation of the flapping angle may be written as,

$$\beta(\Psi) = a_0 - a_1 \cos(\Psi) + b_1 \sin(\Psi) \quad (3)$$

where $\Psi = \Omega t$, the bias component a_0 is the coning angle, a_1 is the longitudinal flapping angle, b_1 is the lateral flapping angle, and Ω is the rotor angular speed. The stabilizer bar which is a teetering type of rotor has no collective input, hence has no coning flapping angle. The cyclic inputs of the Bell-Hiller mixing system may be expressed as,

$$T'_{lat} = \bar{T}_{lat} - b_{1,st} K_h \quad (4)$$

$$T'_{lon} = \bar{T}_{lon} - a_{1,st} K_h \quad (5)$$

where K_h is the Hiller gain which represents the gain from stabilizer bar flapping angle to main rotor pitch, and $b_{1,st}$ and $a_{1,st}$ are the lateral and longitudinal flapping angles of the stabilizer bar. The cyclic blade pitch components \bar{T}_{lat} and \bar{T}_{lon} may be reconstructed by finding the inverse of (1) to obtain \mathbf{T} , and then finding the (linear) mapping to \mathbf{T} .

The rotor flapping dynamics are obtained by writing the torque balance equation for the blade about the flapping point,

$$I_b \ddot{\beta} = \sum_i \tau_i \quad (6)$$

where I_b is the blade moment of inertia about the flapping hinge. The torque components that are contained in the the model are listed below. Equations are introduced (restated from Hald et al. (2006)) for torque components that are a function of parameters that are relevant for system identification.

- **Aerodynamic torque** Generated by the aerodynamic lift for blade element dL given by

$$d\tau_{aero} = r dL \quad (7)$$

where

$$dL = \frac{1}{2} \rho C_l c V_b^2 dr, \quad (8)$$

dL is the elemental lift equation derived from *blade element theory*, r is the displacement from the hinge axis, C_l is the coefficient of lift, ρ is the air density, c is the chord length of the blade, and V_b is the blade velocity with respect to the air.

- **Restraint torque** The torque due to the restoring force caused when the blade flaps, is

$$\tau_{res} = K_s \beta \quad (9)$$

where K_s is the virtual hinge spring constant, and β is the flapping angle.

- **Centrifugal torque** The differential torque due to the centrifugal force that results when the blades rotate is given by

$$d\tau_{cf} = r dF_{cf} \sin(\beta) \quad (10)$$

where

$$dF_{cf} = -\Omega^2 (e + r \cos(\beta)) dM_b, \quad (11)$$

e is the displacement between the center of rotation and the virtual hinge, dM_b is the mass of a differential blade element.

- **Body angular torque** An angular acceleration of the body gets reflected as a linear acceleration of blade elements which result in torque on the blade about the hinge axis.

- **Body normal torque** The body normal torque is the torque on the blade with respect to the hinge due to body normal acceleration.
- **Coriolis torque** A torque due to a fictitious force that is apparent when a particle moves in a rotating frame of reference.

The restraint torque is the only component that is non-existent in the stabilizer bar model because it is a teetering rotor. After all torque components have been computed for the length of the blade, the higher-order trigonometric functions are approximated using first-order harmonics. The second-order dynamics for coning, lateral and longitudinal flapping are obtained by substituting the second time derivative of (3) into (6). For a full description of the torque components incorporated in the model see Hald et al. (2006). The tail rotor only has a collective input, thus lateral and longitudinal flapping is assumed to be zero. Due to the tail rotor speed being much higher than the main rotor (4.28 times for the T-REX250SE), the coning behaviour for the tail rotor was not modelled as its bandwidth is much higher than the control bandwidth of related channels.

3.3 Force/Torque and Kinematics

The forces and torques generated by the rotor are a result of aerodynamic lift and drag of the blades. The restraint torque is an additional torque that is significant in the main rotor dynamics. To find the total force on the rotor hub, the elemental forces are integrated along the length of the blade and averaged for one revolution. The lateral and longitudinal torque for the main rotor hub is computed by averaging the reflected force at the virtual hinge and restraint torque over one revolution of blade travel. Since there is no cyclic actuation of the tail rotor, only the force and torque about the rotor axis is considered. All the forces and torques of the main and tail rotor are reflected onto the center of mass. The rigid body six degree-of-freedom kinematic equations describe the center of mass body motion as a function of the forces and torques. To avoid the gimbal-lock phenomenon, the body rates are integrated into quaternions to represent the attitude of the helicopter.

4. SYSTEM IDENTIFICATION

System identification is used to estimate unknown parameters in the model. A dynamic model is derived using the appropriate physical laws as a function of the plant parameters (as explained in Section 3). All the significant system dynamics are considered in modelling so that the *model structure* is capable of capturing the salient features of the plant. Due to uncertainty in the dynamic model and parameters, the mathematical model may not match the physical plant satisfactorily using measured parameters. Parameter estimation uses actual plant data to reconcile the mathematical model. By sensibly bounding the parameters to be estimated, one can drive the dynamic model to match the physical plant while retaining the meaning of the physical parameters. The nonlinear least-squares method was used for estimating parameters through Matlab's Optimization Toolbox.

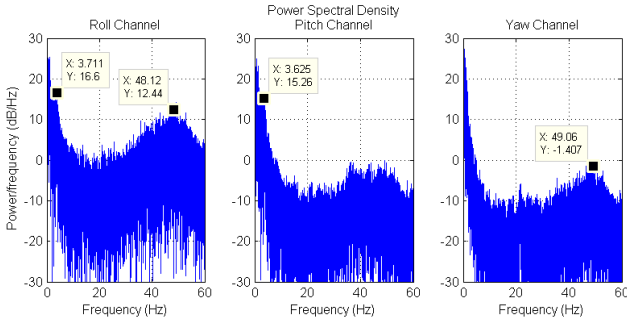


Fig. 6. Power spectral density of the angular rate signals for 10 seconds of hover flight

The servo dynamics were the first to be estimated since it can be easily isolated from the system. A second-order model with rate-limits on the position describe the servo input-to-position dynamics fairly well. For economic reasons, two types of servos are used in RC helicopters. The servos responsible for cyclic control are usually analog and slower compared to the tail collective servo (digital). Step response tests of the servos were logged to identify the parameters that characterise the dynamics. The parameters were found through minimizing the least-square error between simulation and actual step responses. These parameters are given in Table 3.

Table 3. Identified second-order servo parameters

Characteristic	DS410	DS420
Damping ratio, ζ	0.85	0.85
Corner frequency, ω_n (rad/s)	35	45
Rate-limit ($^\circ/s$)	413	672

To get an idea of the bandwidth over which system identification would be necessary, a frequency domain assessment of the plant body kinematics were made. The body angular rates were logged on-board at 200 Hz during a flight. After identifying 10 seconds of hover flight data, a discrete Fourier transform was done for that data. The analysis showed that most of the plant dynamics were under 20 Hz, and there is significant vibration transmission at the motor rotation frequency. The roll channel was found to have the least attenuation of the vibration from the motor. This is not surprising as the smallest inertia is expected to be along the roll axis. Figure 6 shows the power spectral density of the body angular rates for hover flight.

Since the closed-loop bandwidth is expected to be under 20 Hz, the visual tracking system is used to estimate the body linear velocity. For angular velocity measurements, the gyroscopes are used because they have higher accuracy and bandwidth than the visual tracking system. After segments of meaningful data was isolated (hover condition), the data was preprocessed to remove any noise/outliers. The data was then “chopped” into time ranges. The reason for this is because it was found that identification over different time ranges produced an optimal fitting for specific frequency ranges. The underlying problem here is that biased uncertainty in input collective, lateral and longitudinal angles gets mapped to biases in forces and torques on the helicopter body. These signals, once integrated, result in

drift in the body angular and linear velocities. It seems that this is an inevitable challenge in open-loop system identification with high-fidelity models.

Table 4. Uncertain helicopter parameters

Parameter	Interpretation
I_{xx}, I_{yy}, I_{zz}	Moment of inertia about the x, y and z axes
K_{vmr}, K_{hmr}	Center of mass along body xz -plane w.r.t. main rotor
$C_{lmr}, C_{lst}, C_{ltr}$	Lift coefficients for main rotor, stabilizer bar and tail rotor
C_{dmr}, C_{dtr}	Drag coefficient for the main rotor and tail rotor
e_{mr}	Displacement from center of rotation to virtual hinge of main rotor
K_{smr}	Main rotor effective spring constant

The variables shown in Table 4 are difficult to measure, thus formed part of the parameter space across which the optimisation took place. Initial values of parameters were chosen based on laboratory measurements and estimation using CAD models (for the case of inertia). Due to uncertainty in input mapping, a gain and bias term was added to the parameter space for each servo input. Due to the physical plant not having much damping in the yaw dynamics, input uncertainty in tail collective angle easily gets propagated to yaw rate drift. To compensate for this, a low-gain proportional-integral (PI) controller is used to additionally drive the tail rotor collective angle so that the simulation body yaw rate output converges to the physical plant output. Lastly, the initial conditions for the rotor dynamics were added to the set of parameters to estimate.

The time-domain simulation results superimposed over the flight data for body rates over 10 seconds is shown in Fig. 7. Poor approximation of the higher frequency dynamics in the pitch channel can be seen. The least-squares error approach to parameter estimation produced results that lost high bandwidth accuracy with increased

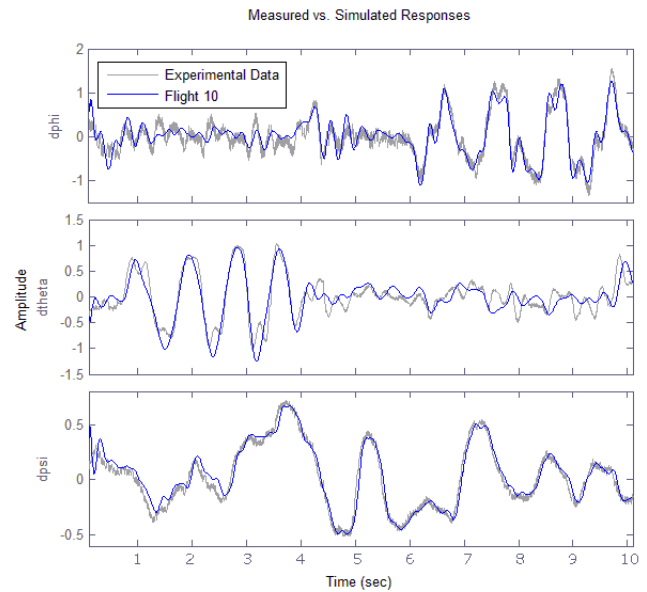


Fig. 7. Simulation output and flight data for roll/pitch/yaw rates (dphi/dtheta/dpsi) (rad/s) for 10 seconds-parameters optimise lower frequency characteristics

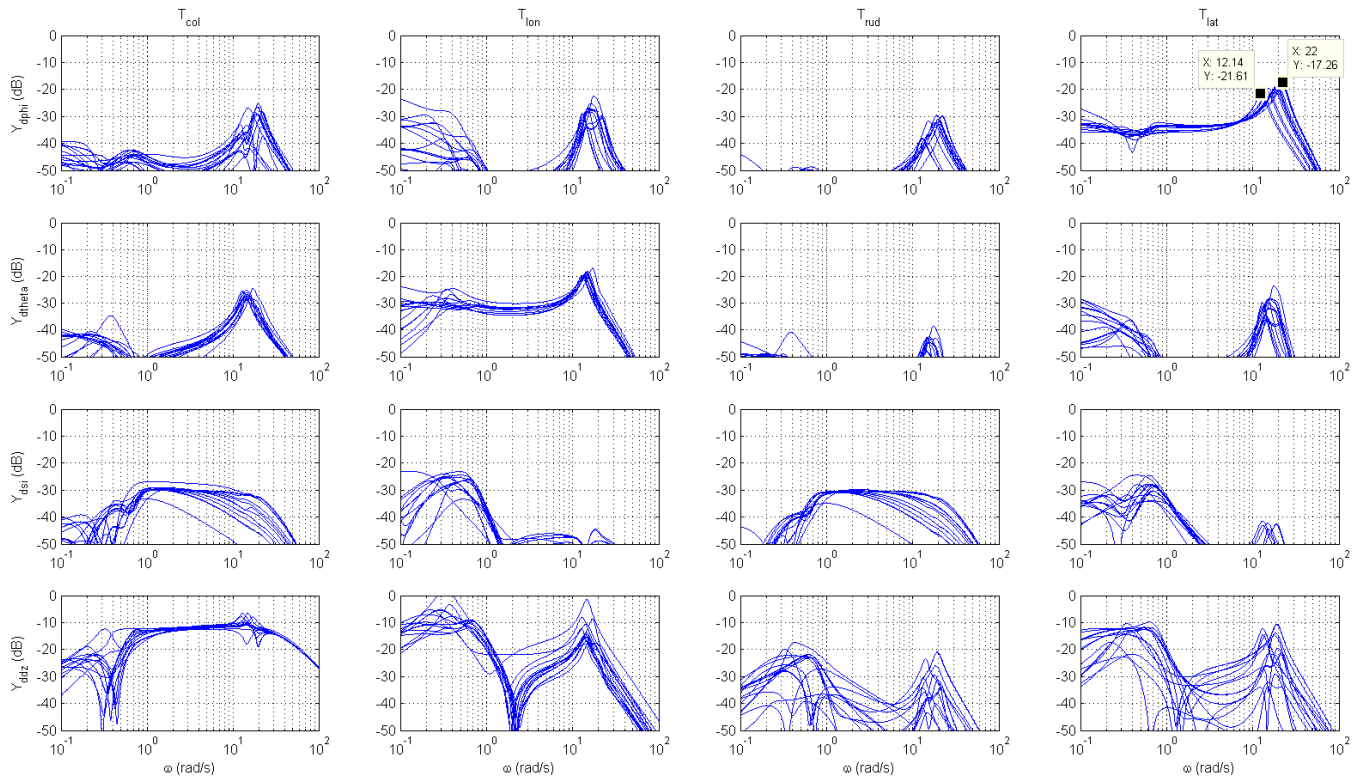


Fig. 8. Bode plot of uncertain plant at hover; Inputs are pilot collective, longitudinal, rudder and lateral stick positions (left to right); Outputs are the body angular (roll, pitch, yaw) rate, and the body acceleration in the z -axis (top to bottom)

identification time. The experiments done with lower identification times capture the higher frequency dynamics much better. To obtain a set of linear plants that fully encapsulate the hover condition, the uncertainty set of parameters were formed by taking the union of parameters across all system identification experiments (with differing identification times). A magnitude plot of the uncertain system is shown in Fig. 8. The results show that there is significant cross-coupling across a resonant band between 12–22 rad/s. A comparison between the magnitude plot in Fig. 8 and the frequency domain responses in Mettler et al. (1999) confirms that the general behaviour is correct, and the expected increase in bandwidth with scale reduction.

5. CONCLUSION

The avionics system developed was successfully used to capture relevant helicopter plant inputs and states required for system identification. Using the low-cost motion capture system we were able to estimate the body linear velocity states sufficiently well for system identification. Parameter estimation using nonlinear least-squares method produced parameters that captured the plant dynamics to a high degree of accuracy. The set of parameters that were generated for different identification time ranges is believed to completely define the plant in hover condition. The system identification results are a validation of the mathematical model developed by Hald et al. (2006). The frequency domain analysis of the approximated system shows that there is significant cross-coupling across channels between 12 and 22 rad/s. This also suggests that a non-diagonal controller design method such as in Boje

(2002) may be suitable to maximise the bandwidth of the system.

REFERENCES

- Bernard, M. and Kondak, K. (2009). Generic slung load transportation system using small size helicopters. In *Robotics and Automation, 2009. ICRA'09. IEEE International Conference on*, 3258–3264. IEEE.
- Bisgaard, M., Bendtsen, J.D., and Cour-Harbo, A.L. (2009). Modeling of generic slung load system. *Journal of guidance, control, and dynamics*, 32(2), 573–585.
- Boje, E. (2002). Non-diagonal controllers in MIMO quantitative feedback design. *International Journal of Robust and Nonlinear Control*, 12(4), 303–320.
- Ducard, G. and D'Andrea, R. (2009). Autonomous quadrotor flight using a vision system and accommodating frames misalignment. In *Industrial embedded systems, 2009. SIES'09. IEEE international symposium on*, 261–264. IEEE.
- Hald, U.B., Hesselbæk, M.V., and Siegumfeldt, M. (2006). *Nonlinear modeling and optimal control of a miniature autonomous helicopter*. Aalborg University.
- Mellinger, D., Michael, N., Shomin, M., and Kumar, V. (2011). Recent advances in quadrotor capabilities. In *Robotics and Automation (ICRA), 2011 IEEE International Conference on*, 2964–2965. IEEE.
- Mettler, B., Tischler, M.B., and Kanade, T. (1999). System identification of small-size unmanned helicopter dynamics. In *Annual Forum Proceedings- American Helicopter Society*, volume 2, 1706–1717.